Development of a New Quantification Method Using Partial Volume Effect Correction for Individual Energy Peaks in ^{111}In-pentetreotide SPECT/CT

Kosuke Yamashita
the Cancer Institute Hospital of JFCR https://orcid.org/0000-0003-0133-7441
Noriaki Miyaji
the Cancer Institute Hospital of JFCR
Kazuki Motegi
the Cancer Institute Hospital of JFCR
Takashi Terauchi
the Cancer Institute Hospital of JFCR
Shigeki Ito (shigekii@kumamoto-u.ac.jp)
Faculty of Life Science, Kumamoto University, 4-24-1 Kuhonji, Chuo-Ku, Kumamoto

Original research

Keywords: Single photon emission computed tomography (SPECT), 111In-pentetreotide, somatostatin receptor scintigraphy (SRS), indium uptake index (IUI), partial volume effect (PVE), energy peak

Posted Date: September 17th, 2021

DOI: https://doi.org/10.21203/rs.3.rs-877512/v1

Abstract

Background

Somatostatin receptor scintigraphy (SRS) using ^{111}In-pentetreotide has no established quantification method. The purpose of this study was to develop a new quantitative method to correct the partial volume effect (PVE) for individual energy peaks in ^{111}In-pentetreotide single-photon emission computed tomography (SPECT).

Methods

Phantom experiments were performed to construct a new quantitative method. In the phantom experiments, a NEMA IEC body phantom was used. Acquisition was performed using two energy peaks (171 keV and 245 keV) on the SPECT/CT system. In the SPECT images of each energy peak, the region of interest was set at each hot sphere and lung insert, and the recovery coefficient (RC) was calculated to understand the PVE. A new quantitative index, the indium uptake index (IUI), was calculated using the RC to correct the PVE. The quantitative accuracy of the IUI in the hot sphere was confirmed. Case studies were performed to clarify the quantitative accuracy. In a case study, the relationship between the IUI and the Krenning score, which is used as a visual assessment, was evaluated for each lesion.

Results

The obtained RCs showed that the energy peak at 171 keV was faster in recovering the effect of PVE than that at 245 keV. The IUI in the 17 mm diameter hot sphere was overestimated by 3.1% at 171 keV and underestimated by 0.5% at 245 keV compared to the actual IUI. In case studies, the relationship between IUI and Krenning score was rs = 0.805 ($p < 0.005$) at sum, rs = 0.77 ($p < 0.005$) at 171 keV, and rs = 0.84 ($p < 0.005$) at 245 keV.

Conclusion

We have developed a new quantification method for ^{111}In-pentetreotide SPECT/CT using RC-based PVE correction for an individual energy peak of 171 keV. The quantitative accuracy of this method was high even for accumulations of less than 20 mm, and it showed a good relationship with the Krenning score; therefore, the clinical usefulness of IUI was demonstrated.

1. Background

Neuroendocrine neoplasm (NEN) is a rare disease that occurs in 2.5% of every 100,000 people [1]. However, the number of patients with this disease is increasing every year [2]. Recently, not only computed tomography (CT) and magnetic resonance imaging (MRI) for morphological diagnosis, but also nuclear medicine examinations using ^{111}In-pentetreotide (somatostatin receptor scintigraphy; SRS) is used for the functional diagnosis of NEN [3]. ^{111}In-pentetreotide binds specifically to subtypes 2, 3, and

5 of the somatostatin receptors (SSTR), which occur frequently and accumulate in NEN, and the accumulation is visualized by a gamma camera [4]. Thus, SRS is recommended for use in local diagnosis, metastasis diagnosis, and confirmation of somatostatin receptor expression [5]. In addition, peptide receptor radionuclide therapy (PRRT) with a similar mechanism has already been performed by synthesizing the radionuclides ^{177}Lu and ^{90}Y using a ligand similar to ^{111}In-pentetreotide [6]. SRS is an important examination to confirm the amount of somatostatin receptors, which affect the efficacy of treatment with PRRT, and can contribute to theranostics expected in the field of nuclear medicine in the future [7]. Since no quantitative method has been established for SRS, the Krenning score, which is a visual evaluation, is commonly used [8]. ^{177}Lu has a physical half-life of 6.7 days byβ- decays (0.498 MeV, 78%), emitting γ-rays (208 keV: 11%) [9]. In clinical trials using ^{177}Lu-DOTA-TATE, the standard of care is to treat patients with a Krenning score of 2 or higher in SRS [10]. The Krenning score is a subjective visual score that may not be reproducible [11]. Therefore, a quantitative method for ^{177}Lu SRS is required for clinical studies to improve the quality of diagnosis.

In an epidemiological study of NENs conducted by Ito et al., a significant correlation ($p = 0.01$) was found between tumor size (> 1 cm) and lymph node metastasis, making it clinically important to identify NENs larger than 1 cm [12]. However, in SRS, it is difficult to accurately assess the activity of tumors smaller than 2 cm because of the partial volume effect (PVE) caused by the resolution of single-photon emission computed tomography (SPECT) [13]. Several methods using the recovery coefficient (RC) have been developed to improve the image resolution in SPECT images [14]. Additionally, the PVE correction method has been used to improve the accuracy of quantification [15]. By applying RC and PVE corrections to the SRS-SPECT, accurate quantitative values can be obtained even for small lesions.

The energy window setting is also an important factor for SPECT imaging, as it affects the quantitative accuracy [16]. ^{111}In, which has a physical half-life of 2.8 days, decays by orbital electron capture, emitting γ-rays (171 keV: 90.2%, 245 keV: 94.0%) and characteristic X-rays (Kα: 23.1 keV, 69.0%; Kβ: 26.2 keV, 14.1%) [17, 18]. In the case of bone scintigraphy, it has been reported that the quantification accuracy is improved by optimizing the energy window [19]. For the SRS-SPECT, the two energy peaks, 171 and 245 keV, are commonly used for imaging [20]. Because these peaks have different counting efficiencies of the gamma camera as well as different collimator penetration, scattering correction accuracy, and counting volume, there is a concern that the use of a combined energy window would affect the accuracy of the quantification [21]. A more accurate quantification method for SRS can be developed by correcting the PVE by using RC for individual energy peaks. Moreover, this method can be applied to ^{177}Lu-SRS.

Therefore, the purpose of this study was to develop a new quantification method with accuracy by PVE correction, using RC for individual energy peaks calculated by phantom in ^{111}In-pentetreotide SPECT.

2. Methods

2.1. SRS imaging protocol

All images were acquired on a Symbia Intevo 16 (Siemens Medical Solution, Erlangen, Germany) with low middle-energy general purpose (LMEGP) collimators. The energy windows for ^{111}In-SPECT were selected as 172 keV ± 7.5% and 247 keV ± 7.5% for the main window, 15% and 8% for the lower and upper windows of 172 keV, respectively, and 10% for the lower window of 247 keV (Fig. 1). SPECT scan was performed for 20 min (60 steps, 40 s/step, 128×128 matrix; magnification, 1.0; pixel size, 4.8 mm). SPECT images were obtained using the ordered subset expectation maximization (OSEM) method (Flash3D; Siemens Healthcare, Erlangen, Germany) with 12 iterations and 6 subsets. Images were smoothed using a Gaussian filter (9.6 mm at full width half maximum). Scattering correction was performed using the triple energy window (TEW) method at 171 keV and dual energy window (DEW) method at 245 keV. Attenuation correction was performed using computed tomography attenuation correction (CTAC). CT acquisition for attenuation correction was performed using adaptive dose modulation (CARE Dose 4D; Siemens Healthcare, Erlangen, Germany) at a tube voltage of 130 kV and tube current of 80 mA. The CT data were reconstructed to a slice thickness of 3 mm, and medium sharp and attenuation kernels (B50s and B31s, respectively) were used. All image analyses were performed using the Daemon Research Image Processor (DRIP; Fujifilm Toyama Chemical Co., Ltd., Tokyo, Japan) version 3.0.2.0, and OsiriX software (Pixmeo, Bernex, Switzerland) v. 12.0.3.

2.2. Phantom studies

2.2.1. Phantom design

The characteristics of each energy peak were confirmed by phantom experiments. A NEMA IEC body phantom (Data Spectrum, NC, USA) was used to simulate the upper abdomen. Six hot spheres (φ37, 28, 22, 17, 13, and 10 mm) and lung insert (φ44 mm) were placed in the phantom. The renal excretion rate of ^{111}In-pentetreotide in the human body after 24 h is 85%, and the uptake in the upper abdomen relative to the whole body is approximately 60 %–70% [19]. The residual rate of ^{111}In-pentetreotide in the body after 24 h is approximately 20 MBq. Therefore, the entire phantom contained 13 MBq of the ^{111}In solution (Fig. 2).

The cross-calibration factor (CCF), which is necessary to calculate the quantitative value, was measured. A polyethylene bottle (φ95 mm, volume = 1170 mL) was used for the CCF; The bottle was filled with 3.47 kBq/mL of ^{111}In solution for the measurement.

2.2.2. Data analysis

Three types of SPECT images were used: images acquired at 172 keV ± 7.5% and 247 keV ± 7.5% in the main window (171 keV image and 245 keV image, respectively), and images acquired by summing the two windows (sum image). To clarify the PVE, the RC was determined for each window. A new quantitative value, the indium uptake index (IUI), was calculated by correcting the RC.

Regions of interest (ROIs) were placed at the hot spheres and lung insert in the SPECT images for each window, adjusting the position and size with reference to the CT images. The shape of the ROI was a circle that matched the shape of the hot sphere and lung insert. The hot sphere was placed in the slice

where it was most depicted in the three slices, before and after the slice corresponding to the hot sphere of the lung insert (Fig. 3). The maximum counts in the three slices before and after each hot sphere and lung insert were measured from the ROIs. The RCs were calculated as follows:

$$RC = \frac{C_{max,i}}{C_{max,44}}$$

1

$C_{max,44}$ is the maximum count in the lung insert, and $C_{max,i}$ is the maximum count in each hot sphere.

Based on the relationship between the calculated RCs and the diameters of the hot spheres and lung insert, spline interpolation was performed between the measurements to observe a total of 60 RCs using the original program written in Python. Wilcoxon's signed rank sum test was used to examine the differences between the three measured RCs. $P < 0.05$ was considered statistically significant.

To correct the PVE for accumulations of 44 mm or less in diameter, the maximum count of the hot spheres and lung insert must be divided by the RC corresponding to their diameter. In calculating the quantitative value, the dosage and weight of the patient must be considered. The standardized uptake value (SUV) method is commonly used to calculate quantitative values independent of body weight and dose [22]. In this study, the IUI was calculated with reference to this method. The IUI of each hot sphere and lung insert was calculated as follows:

$$IUI = \frac{\frac{C_{maxi,energy}}{RC_{i,energy}}}{Doseradioactivity(Bq) / Weight(g)} \times CCF$$

2

$C_{max\ i,energy}$ is the maximum count of each hot sphere in each window, $RC_{i,energy}$ is the RC corresponding to the diameter in each window, *Dose radioactivity* is the amount of radioactivity actually contained in the phantom (Bq), and *Weight* is the weight of the phantom (g). *CCF* is calculated from the radioactivity concentration in the bottle and the counts from the SPECT images.

In this study, 17 mm spheres were measured to confirm the quantitative accuracy for accumulations of less than 20 mm in diameter. The quantitative values for the 17 mm sphere were calculated using two patterns: IUI and SUV. In addition, the percentage (%) difference was calculated to confirm the difference between the ideal quantitative value and calculated quantitative value. The %difference was calculated as follows:

$$\%difference = \frac{Index_{ref} - Index_{cal}}{Index_{ref}} \times 100$$

3

$Index_{ref}$ is the ideal quantitative value of IUI and SUV (IUI, SUV = 8.8), and $Index_{cal}$ is the quantitative value of IUI and SUV by calculation.

2.3. Case study

2.3.1. Patient protocol

All patients underwent SRS at the Cancer Institute Hospital of JFCR between April 2016 and March 2020. Fourteen patients (17 sites) were included in the study. Four patients had normal liver metastases, seven had liver metastases (two pancreatic tumors), and five had pancreatic head and body tumors (two liver metastases). In all patients, ^{111}In-pentetreotide (Octreoscan; Fujifilm Toyama Chemical Co., Ltd., Tokyo, Japan) was administered at a dose of 180.1 ± 14.8 MBq. The selection criteria for patients were as follows: at least one SPECT/CT session performed 24 hours after ^{111}In-pentetreotide administration, no liver lesions on modalities other than SPECT/CT in patients with normal liver, and no accumulation of lesions on SPECT/CT in patients with liver metastases or pancreatic head or body tumors. In cases of liver metastases and pancreatic head and body tumors, SPECT/CT showed accumulation in the lesions.

2.3.2. Data analysis

The IUI was calculated for all 17 sites using the RC and CCF calculated by the phantom experiments.

For the calculation of IUI in normal liver cases, ROIs of a size that enclosed the liver were placed visually in the liver area of the case images (Fig. 4). The IUI in the liver region was calculated for each window using the obtained maximum count, dose for each case, and body weight.

For the accumulation of liver metastases and tumors in the head and body of the pancreas, ROIs were set according to the size of the tumor, and the maximum counts in the tumor were measured (Fig. 5). Tumor size was measured using the previous CT and MRI. Based on the measured length and diameter of each tumor, the RC was selected, and the IUI was calculated using the maximum count.

Table 1
Definition for Krenning score (0–4)

Score	Intensity
0	None (no uptake)
1	Very low
2	Less than or equal to that of the liver
3	Greater than that of the liver
4	Greater than that of the spleen

Krenning scores for all sites were determined according to Table 1. For cases with normal liver, the score was set to 2 based on the criteria of the Krenning score. The correlation coefficient was used to clarify the relationship between the Krenning score and IUI.

2.4.3. Statistical analysis

To check for differences between the groups, Friedman's test was used for the calculated IUI for each energy window. To clarify the relationship between the Krenning score and IUI, box plot analysis was used, and Spearman's rank correlation coefficient was calculated. Statistical significance was set at $p < 0.05$. All statistical analyses were performed using Easy R (Saitama Medical Center, Jichi Medical University, Saitama, Japan) version 1.54, and the graphical user interface of R (The R Foundation for Statistical Computing, Vienna, Austria) version 3.6.2 [23].

3. Results

3.1. Phantom studies

A trans-axial image collected in each window is shown in Fig. 5. Compared to the 171 keV image, the 245 keV image shows relatively more noise and a small number of counts around the phantom. In addition, the 171 keV image had the highest image quality, and the accumulation of each hot sphere was circular.

The spline interpolated graphs of the RCs obtained from the NEMA IEC body phantoms for each window are shown in Fig. 6. The RCs of the 13 mm and 10 mm spheres were almost the same owing to the PVE. At 171 keV, the RC reached approximately 1.0, at a sphere size of 37 mm, but did not reach 1.0 until 44 mm for the other windows. There was a significant difference between the three RC curves ($p < 0.005$).

Table 2 shows the % difference in IUI and SUV for the 17 mm diameter hot sphere in each window. By using RC, the difference in IUI between the energy peaks was almost eliminated. While the SUVs were underestimated by more than 50%, the IUI at sum, 171 keV, and 245 keV were almost the same as the IUI = 8.8 calculated from the actual radioactivity, but were overestimated by 3.1% at 171 keV and underestimated by 0.5% at 245 keV.

Table 2
Difference (%) between IUI, SUV of each window and ideal IUI, SUV (IUI, SUV = 8.8) for lung insert (φ17mm)

Energy window	IUI	% difference	SUV	% difference
171keV	9.07	+ 3.1%	3.85	-56.2%
245keV	8.75	-0.5%	3.16	-64.0%
sum	8.97	+ 2.0%	3.81	-56.7%

An example of a case image for each window is shown in Fig. 7. Similar to the results of the phantom experiment, the images using 245 keV showed slight counts along the body surface and bed.

Finally, the relationship between IUI and Krenning score in each window is shown in Fig. 8. There was no significant difference in the IUI between the three groups in each window ($p = 0.161$). The relationship between IUI and Krenning score showed a good correlation in each window (sum: $rs = 0.805$, $p < 0.005$; 171 keV: $rs = 0.77$, $p < 0.005$; 245 keV: $rs = 0.84$, $p < 0.005$).

4. Discussion

We have developed a new quantification method for ^{111}In-pentetreotide SPECT using PVE correction with RC values at individual energy peaks determined by phantom experiments.

This study showed that each energy peak of ^{111}In has various characteristics. In particular, the shape of the RC curve and the size of the accumulation above 1.0 are different for the two peaks, and they have different characteristics of the PVE. In a previous report, the PVE was not affected when the size of the accumulation was more than twice the system resolution [24]. The system resolution of the LMEGP collimator used in this study was 10.4 mm, which means that the PVE was not affected if the accumulation was approximately 21 mm [25]. However, the RC did not reach 1.0 until 44 mm in diameter at 245 keV. Holstensson et al. and Noori-Asl et al. confirmed the effect of scattering correction at 171 keV and 245 keV in simulations and phantom experiments and reported that the removal rate of scattered radiation was different between 171 keV and 245 keV [21, 26]. In addition, the energy at 5% septal penetration of the LMEGP collimator is 240 keV, and the second energy peak of the ^{111}In used (245 keV) was higher [25]. The penetration of the energy peak at 245 keV is expected to be more than 5% in the image. In cerebral blood flow using SPECT with ^{123}I-IMP, it has been reported that penetration increased the variation in quantitative values [27]. Therefore, when the LMEGP collimator was used, the RC was affected by the scattering rejection rate and penetration at the 245 keV energy peak. This result may be a factor that degrades quantification accuracy. Although IUI could provide high quantitative accuracy regardless of the energy peak, the effect of the 245 keV penetration was very pronounced in SPECT images. Mahler et al. reported that penetration using extended low-energy general purpose (ELEGP) was greater than that using collimators for medium energy general purpose (MEGP) [28]. Therefore, it is reasonable to use only the 171 keV energy peak for IUI in ^{111}In-pentetretoide SPECT to improve the quantitative accuracy and delineation performance.

Currently, there are many reports on the use of SUV in bone SPECT examinations [29]. SUV has the problem of PVE, which is limited by the inherent system resolution of the device, and it is difficult to calculate accurate quantitative values [30]. Tran-Gia et al. performed PVE correction using RC in ^{177}Lu-SPECT and reported its usefulness [14]. Applying the same method to SRS-SPECT, the IUI simply reduces the PVE inherent to gamma cameras. It has been reported that the quantitative accuracy of bone SPECT is within 3% by improving the accuracy of various corrections [32]. The quantitative accuracy of SRS is

of the lower dose. However, in a phantom experiment

simulating the actual dose, the IUI was able to establish a quantitative accuracy of approximately 3%, suggesting the usefulness of PVE correction using RC.

In the case study, there was a good relationship between IUI and Krenning score, indicating the clinical usefulness of IUI. The Krenning score has been used in clinical trials of therapeutic agents such as PRRT and lanreotide [6, 32]. The Krenning score has also been reported to be a strong indicator of the therapeutic effect of PRRT [33]. Therefore, it may be difficult for the IUI to replace the Krenning score. In this study, the IUI showed a wide range of values for each Krenning score and was able to subdivide the characteristics of the lesions. Therefore, IUI should be used as a complement to the Krenning score.

These results suggest that IUI is a clinically useful tool for improving the quality of diagnosis using ^{111}In-pentetreotide SPECT. In addition, the fact that the IUI can be calculated simply and without the need for special devices is one of the greatest advantages of this quantitative method, and we believe that it is feasible to verify the proposed quantitative method in a large-scale multicenter study.

In this study, the ME collimator used in ^{111}In-pentetreotide SPECT was not examined. In ^{111}In-pentetreotide SPECT, the difference in delineation performance between ME general purpose (MEGP), ELEGP, and low energy general purpose (LEGP) has been reported [28]. The characteristics of the energy peaks are expected to differ from those of LMEGP. The use of IUI in the case of the ME collimator is a matter for further study.

All IUIs were calculated using a manual ROI setting, where the ROI setting position differs each time, and the reproducibility of quantitative values cannot be maintained. Therefore, it is expected that the development of an automatic ROI setting program will improve not only the reproducibility but also the analysis efficiency of the proposed IUI calculation, and it is necessary to further study this issue.

5. Conclusion

We developed a new quantification method for ^{111}In-pentetreotide SPECT. This method has high quantification accuracy even for accumulations of less than 20 mm by PVE correction using RC for an individual energy peak of 171 keV. In addition, the IUI has a good correlation with the Krenning score, which has been used in the past, and is expected to be used as a complementary method to the Krenning score in the future.

Abbreviations

PVE partial volume effect

SPECT single photon emission computed tomography

RC recovery coefficient

NEN neuroendocrine neoplasm

SRS somatostatin receptor scintigraphy

SSTR somatostatin receptor

PRRT peptide receptor radionuclide therapy

LMEGP low middle energy general purpose

OSEM ordered subsets expectation maximization

TEW triple energy window

DEW dual energy window

CTAC computed tomography attenuation correction

DRIP daemon research image processor

ROI regions of interest

CCF cross-calibration factor

SUV standardized uptake value

ELEGP extended low energy general purpose

MEGP medium energy general purpose

LEGP low energy general purpose

Declarations

Ethics approval and consent to participate

The Ethics Committee at the Cancer Institute Hospital of JFCR approved this clinical study (approval no. 2020-1171). The results of this retrospective study did not influence any further therapeutic decision-making.

Consent for publication

Not applicable

Availability of data and material

udy are included in this published article.

Competing interests

The authors declare that they have no competing interests.

Funding

None

Authors' contributions

KY contributed to the study design, phantom data acquisition, and data analysis. NM and SI contributed to the study design, data analysis, and drafting and critical revision of the manuscript. TT and KM contributed to the critical revision of the manuscript. All authors read and approved the final manuscript.

Acknowledgements

We would like to thank the staff of the Diagnostic Imaging Center at the Cancer Institute Hospital of JFCR.

References

1. Modlin IM, Lye KD, Kidd M. A 5-decade analysis of 13,715 carcinoid tumors. Cancer. 2003;97:934–59.
2. Yao JC, Hassan M, Phan A, Dagohoy C, Leary C, Mares JE, et al. One hundred years after “carcinoid”: Epidemiology of and prognostic factors for neuroendocrine tumors in 35,825 cases in the United States. J Clin Oncol. 2008;26:3063–72.
3. Zuetenhorst JM, Taal BG. Metastatic Carcinoid Tumors: A Clinical Review. Oncologist. 2005;10:123–31.
4. Kubota K. PET and SPECT for neuroendocrine tumor. Off. J. Japan Assoc. Endocr. Surg. Japanese Soc. Thyroid Surg. 2015;32:112-5.
5. Kwekkeboom DJ, Krenning EP, Scheidhauer K, Lewington V, Lebtahi R, Grossman A, et al. ENETS Consensus Guidelines for the Standards of Care in Neuroendocrine Tumors: Somatostatin Receptor Imaging with 111In-Pentetreotide. Neuroendocrinology. 2009;90:184–9.
6. Strosberg J, Wolin E, Chasen B, Kulke M, Bushnell D, Caplin M, et al. Health-related quality of life in patients with progressive midgut neuroendocrine tumors treated with 177 lu-dotatate in the phase III netter-1 trial. J Clin Oncol. 2018;36:2578–84.
7. Öberg K. Molecular imaging radiotherapy: Theranostics for personalized patient management of neuroendocrine tumors (NETs). Theranostics. 2012;2:448-58.
8. Krenning EP, De Jong M, Kooij PPM, Breeman WAP, Bakker WH, De Herder WW, et al. Radiolabelled somatostatin analogue(s) for peptide receptor scintigraphy and radionuclide therapy. Ann Oncol. 1999;10:S23-9.

9. de Jong M, Breeman WA, Bernard BF, Bakker WH, Schaar M, van Gameren A, et al. [177Lu-DOTA(0),Tyr3] octreotate for somatostatin receptor-targeted radionuclide therapy. Int J Cancer. 2001;92:628-33.
10. Strosberg J, El-Haddad G, Wolin E, Hendifar A, Yao J, Chasen B, et al. Phase 3 Trial of 177 Lu-Dotatate for Midgut Neuroendocrine Tumors. N Engl J Med. 2017;376:125–35.
11. Wetz C, Apostolova I, Steffen IG, Hofheinz F, Furth C, Kupitz D, et al. Predictive Value of Asphericity in Pretherapeutic [111 In] DTPA-Octreotide SPECT/CT for Response to Peptide Receptor Radionuclide Therapy with [177 Lu]DOTATATE. Mol Imaging Biol. 2017;19:437–45.
12. Ito T, Sasano H, Tanaka M, Osamura RY, Sasaki I, Kimura W, et al. Epidemiological study of gastroenteropancreatic neuroendocrine tumors in Japan. J Gastroenterol. 2010;45:234–43.
13. Hope TA, Calais J, Zhang L, Dieckmann W, Millo C. 111In-pentetreotide scintigraphy versus 68Ga-DOTATATE PET: Impact on krenning scores and effect of tumor burden. J Nucl Med. 2019;60:1266–9.
14. Tran-Gia J, Lassmann M. Optimizing image quantification for 177Lu SPECT/CT based on a 3D printed 2-Compartment kidney phantom. J Nucl Med.2018;59:616–24.
15. Finocchiaro D, Berenato S, Grassi E, Bertolini V, Castellani G, Lanconelli N, et al. Partial volume effect of SPECT images in PRRT with 177Lu labelled somatostatin analogues: A practical solution. Phys Med. 2019;57:153-9.
16. Ritt P, Vija H, Hornegger J, Kuwert T. Absolute quantification in SPECT. Eur. J. Nucl. Med. Mol. Imaging. 2011;38 Suppl 1:69-77.
17. Dziel T, Listkowska A, Tymiński Z. Standardisation and half-life measurements of (111)In. Appl Radiat Isot. 2016;109:345-8.
18. A Endo, Y Yamaguchi, , KF Eckerman. Nuclear decay data for dosimetry calculation Revised data of ICRP Publication 38. JAERI 1347. 2005.
19. Koral KF, Clinthorne NH, Leslie Rogers W. Improving emission-computed-tomography quantification by Compton-scatter rejection through offset windows. Nucl Inst Methods Phys Res A. North-Holland; 1986;242:610–4.
20. Bombardieri E, Ambrosini V, Aktolun C, Baum RP, Bishof-Delaloye A, Del Vecchio S, et al. 111In-pentetreotide scintigraphy: Procedure guidelines for tumour imaging. Eur J Nucl Med Mol Imaging. 2010;37:1441-8.
21. Holstensson M, Hindorf C, Ljungberg M, Partridge M, Flux GD. Optimization of Energy-Window Settings for Scatter Correction in Quantitative 111 In Imaging: Comparison of Measurements and Monte Carlo Simulations. Cancer Biother Radiopharm. 2007;22:136-42.
22. Huang SC. Anatomy of SUV. Nucl Med Biol. 2000;27:643–6.
23. Kanda Y. Investigation of the freely available easy-to-use software “EZR” for medical statistics. Bone Marrow Transplant .2013;48:452–8.

24. Soret M, Bacharach SL, Buvat I. Partial-Volume Effect in PET Tumor Imaging. J Nucl Med. 2007;48:932–45.
25. Yoneyama H, Tsushima H, Kobayashi M, Onoguchi M, Nakajima K, Kinuya S. Improved detection of sentinel lymph nodes in SPECT/CT images acquired using a low- to medium-energy general-purpose collimator. Clin Nucl Med. 2014;39:1-6.
26. Noori-Asl M. Assessment of four scatter correction methods in In-111 SPECT imaging: A simulation study. J Med Phys. 2020;45:107–15.
27. Du Y, Tsui BMW, Frey EC. Model-based compensation for quantitative 123I brain SPECT imaging. Phys Med Biol. 2006;51:1269–82.
28. Mähler E, Sundström T, Axelsson J, Larsson A. Detecting small liver tumors with 111In-pentetreotide SPECT-a collimator study based on Monte Carlo simulations. IEEE Trans Nucl Sci. 2012;59:47–53.
29. Dickson J, Ross J, Vöö S. Quantitative SPECT: the time is now. EJNMMI Phys. 2019;6:4.
30. Nakahara T, Daisaki H, Yamamoto Y, Iimori T, Miyagawa K, Okamoto T, et al. Use of a digital phantom developed by QIBA for harmonizing SUVs obtained from the state-of-the-art SPECT/CT systems: a multicenter study. EJNMMI Res. 2017;7:53.
31. Armstrong IS, Hoffmann SA. Activity concentration measurements using a conjugate gradient (Siemens xSPECT) reconstruction algorithm in SPECT/CT. Nucl Med Commun. 2016;37:1212–7.
32. Caplin ME, Pavel M, Ćwikła JB, Phan AT, Raderer M, Sedláčkova E, et al. Anti-tumour effects of lanreotide for pancreatic and intestinal neuroendocrine tumours: The CLARINET open-label extension study. Endocr Relat Cancer. 2016;23:191–9.
33. Kwekkeboom DJ, Teunissen JJ, Bakker WH, Kooij PP, De Herder WW, Feelders RA, et al. Radiolabeled somatostatin analog [177Lu-DOTA0, Tyr3]octreotate in patients with endocrine gastroenteropancreatic tumors. J Clin Oncol. 2005;23:2754–62.

Figures

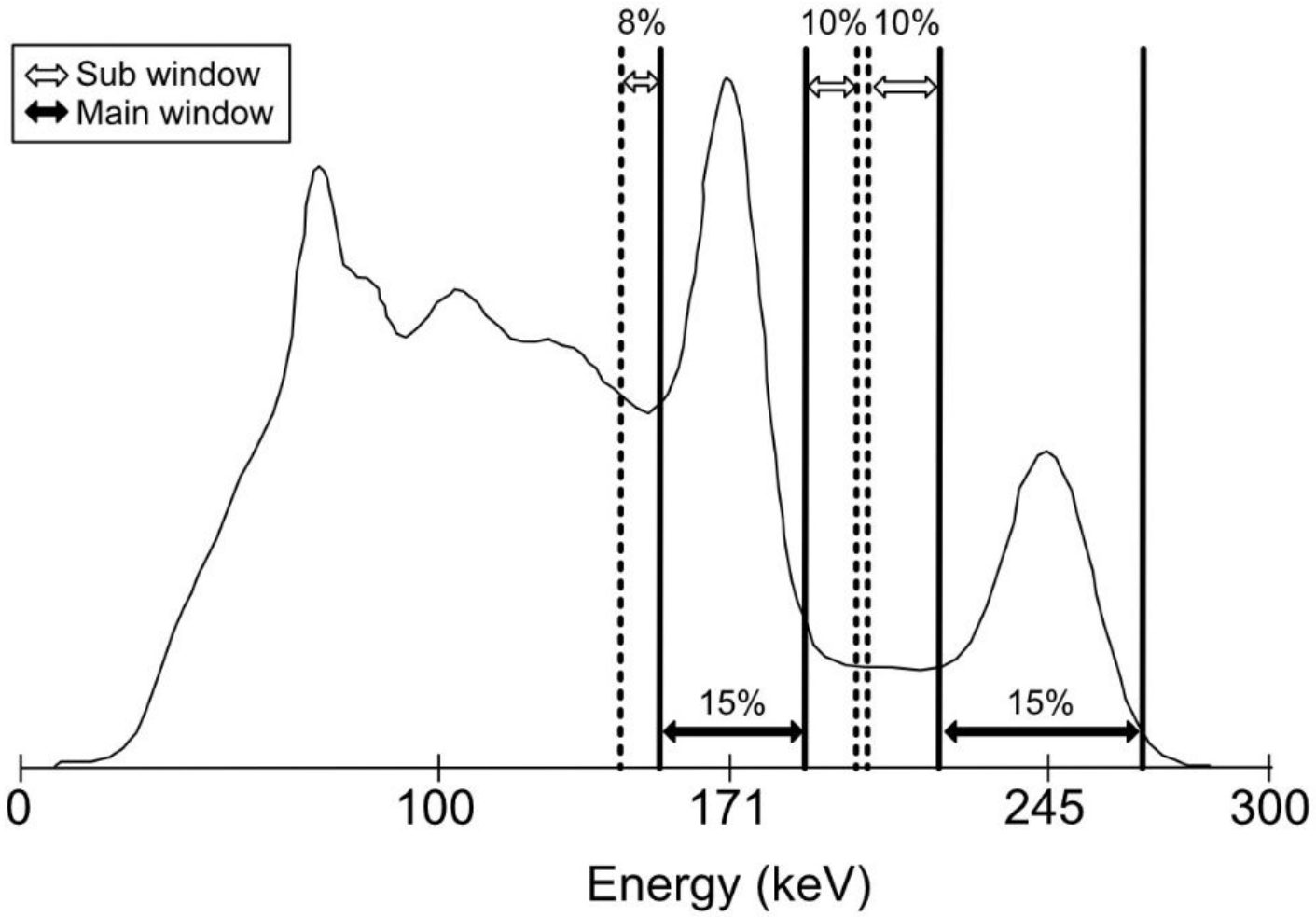

Figure 1

The energy spectrum and window setting of 111In. In this study, the main window (black arrows) of 15% width is opened at the center of 171 keV and 245 keV. The sub-windows (white arrows) of 8% are opened at the lower side and 10% at the upper side of 171 keV, and sub-window of 10% is opened at the lower side of 245 keV.

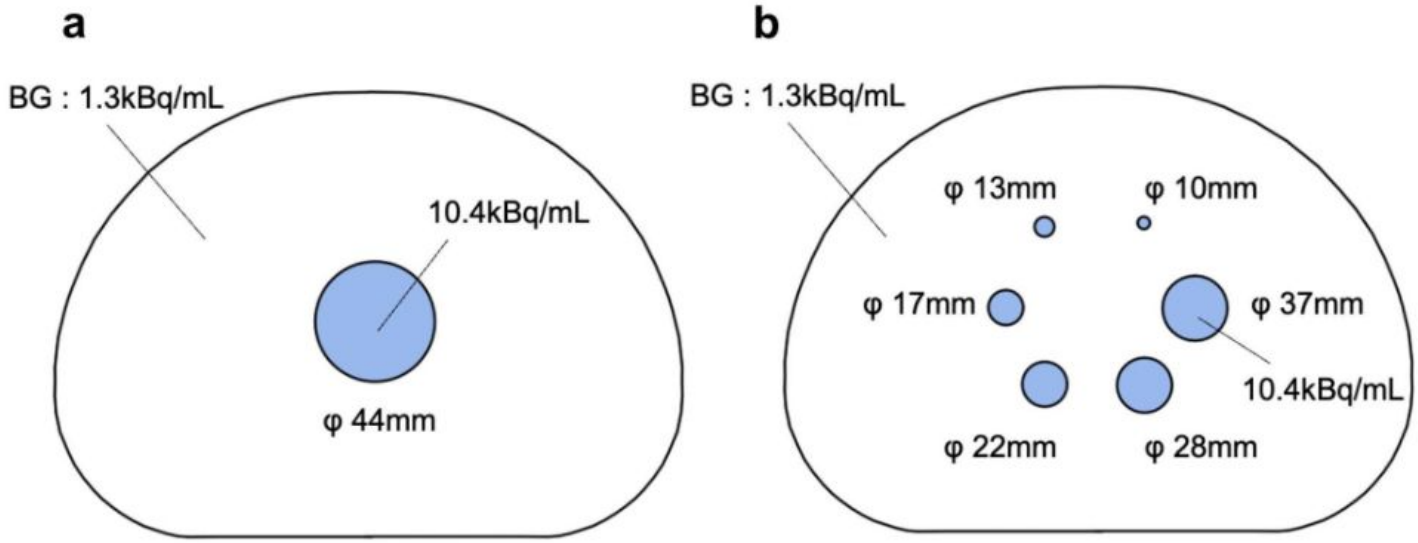

Figure 2

The layouts of the NEMA IEC body phantom. Figure showing the positions of a lung inserts and b hot spheres (φ37, 28, 22, 17, 13, 10 mm) in the NEMA IEC Body phantom. The lung insert is in the center of the phantom and hot spheres are in concentric circles around the center. The dose of the lung insert and hot spheres was 10.4kBq/mL and that of BG was 1.3kBq/mL (TB ratio = 8:1).

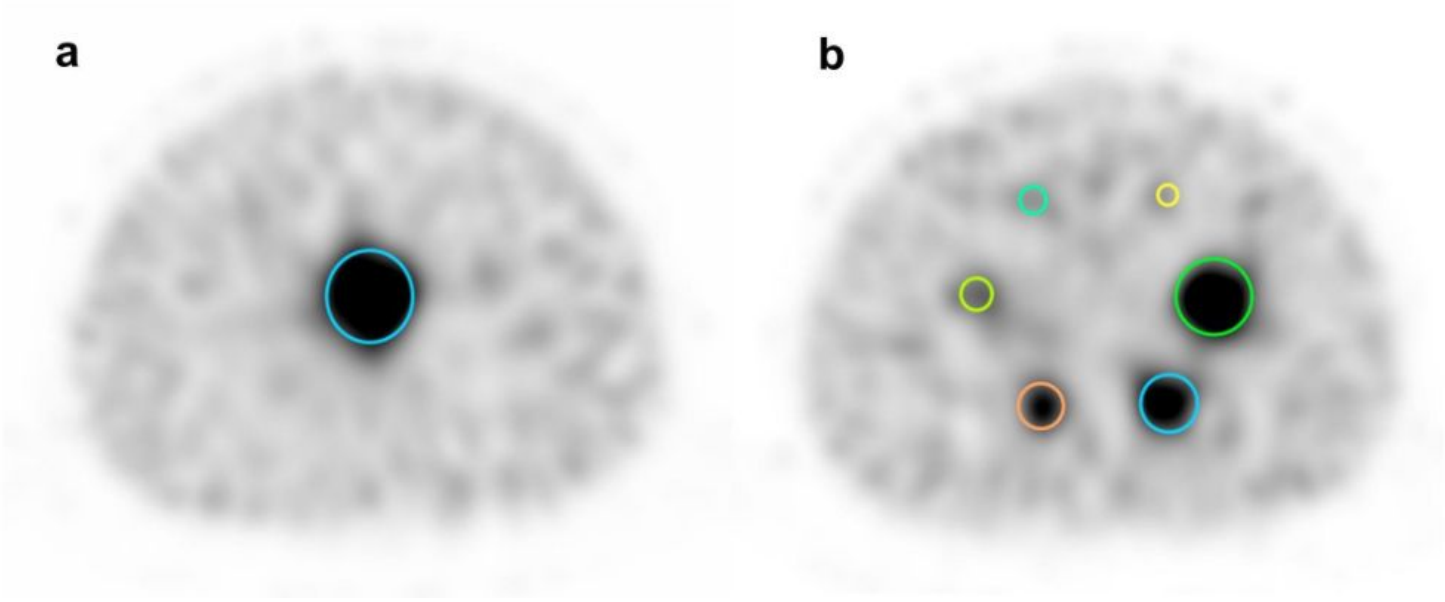

Figure 3

ROI placement in NEMA IEC body phantom. The ROI was set to the slice that was most depicted in the hot spheres (a), and the same slice as the hot sphere in the lung insert (b).

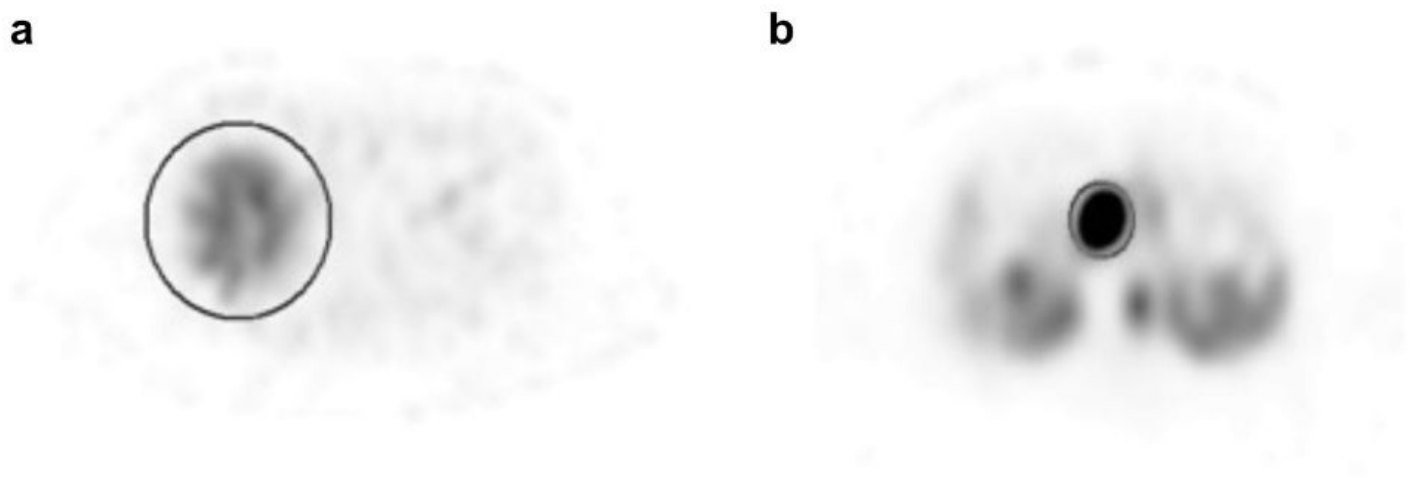

Figure 4

ROI placement in the normal liver and the tumor. The ROI is placed in a uniform location in the upper part of the liver to enclose the entire liver (a). A circular ROI of the same size as the tumor is placed at the maximum depicted slice of the tumor (b).

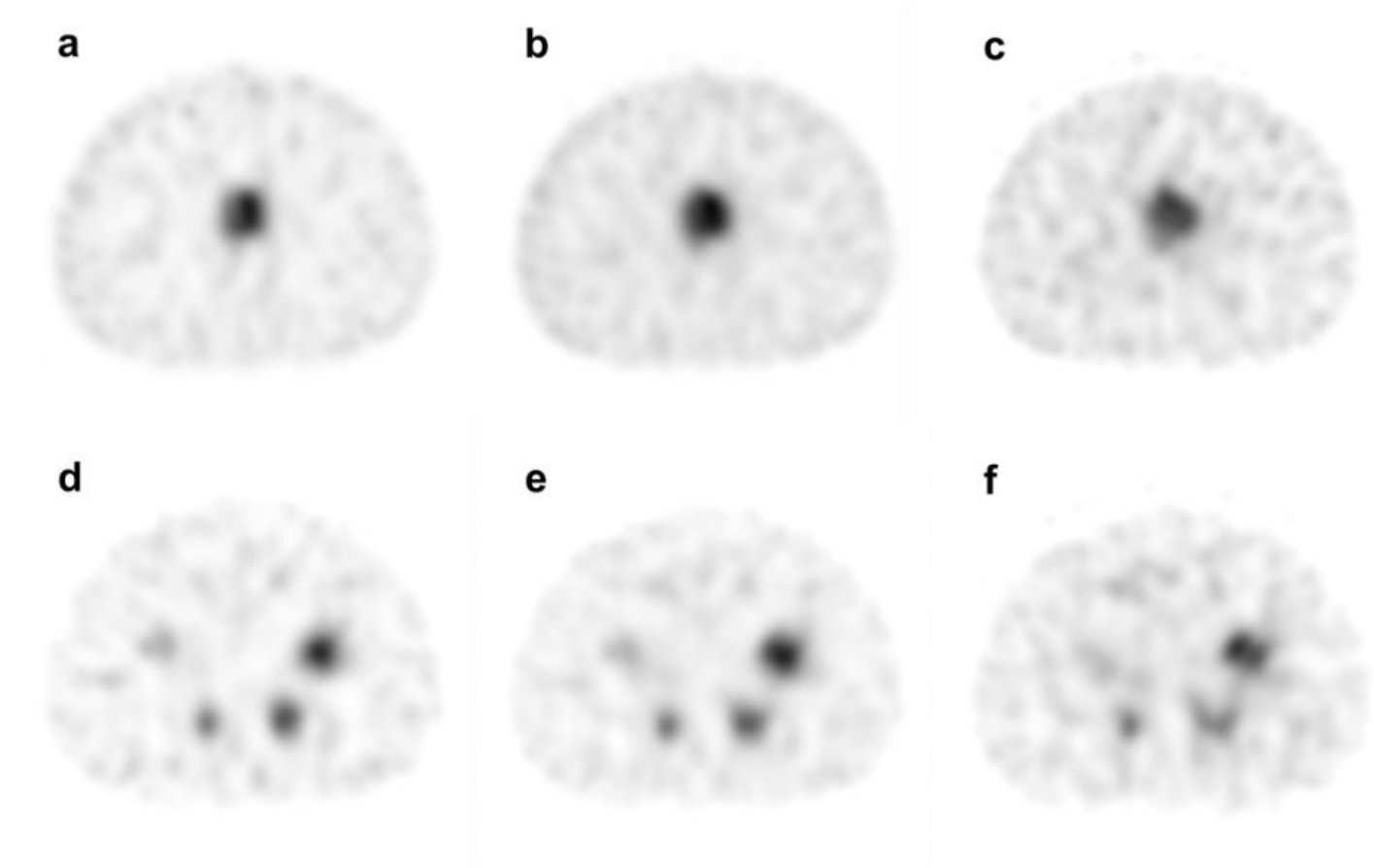

SPECT images of NEMA IEC Body Phantom. Reconstruction was performed for 171 keV (a, d), 245 keV (b, e), and sum (c, f). The upper image shows the lung insert (a, b, c), and the lower image shows the hot spheres (d, e, f).

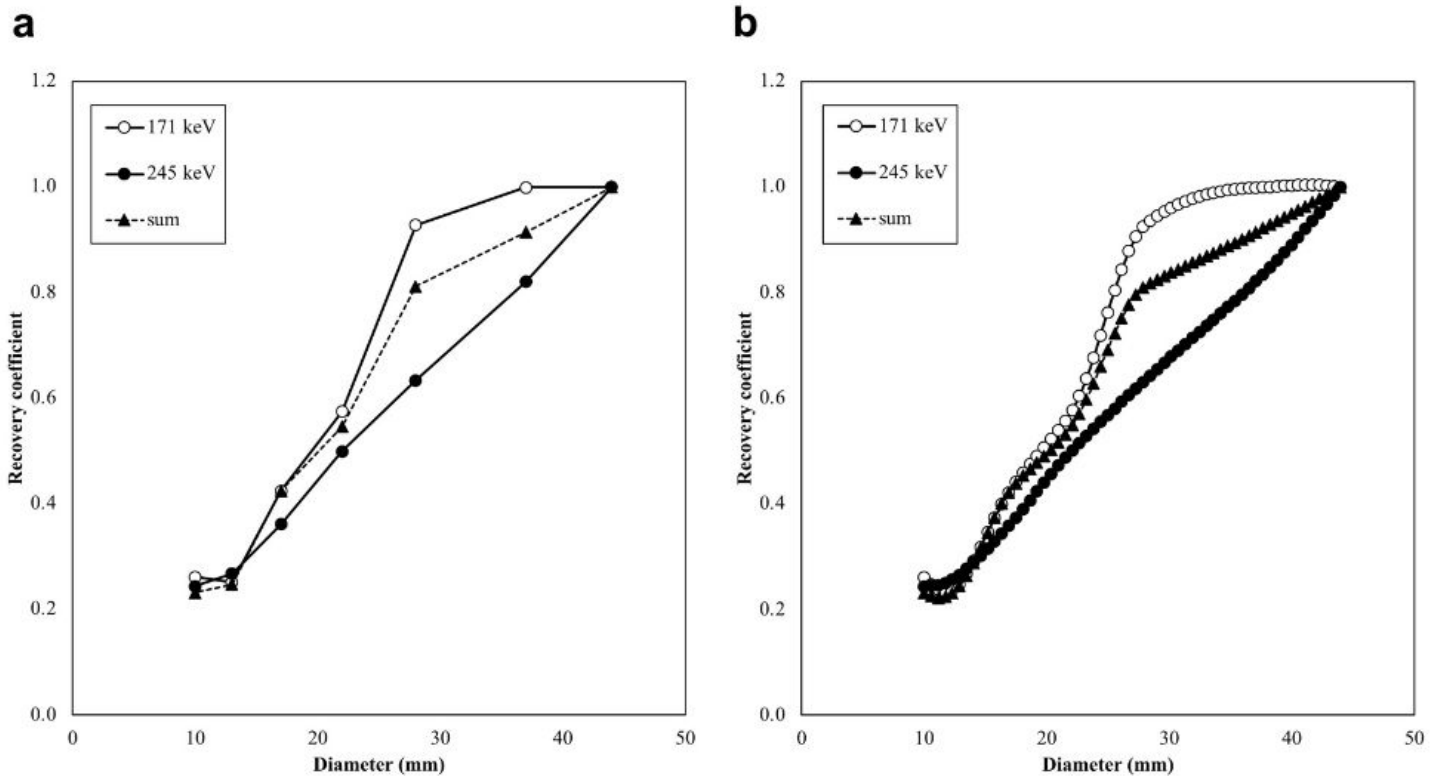

Figure 6

Relationship between the diameter of the accumulation and the RC. a the RC in each hot sphere and the lung insert. b the RC with spline interpolation. Triangles indicate sum, white circles indicate 171 keV, and black circles indicate 245 keV data.

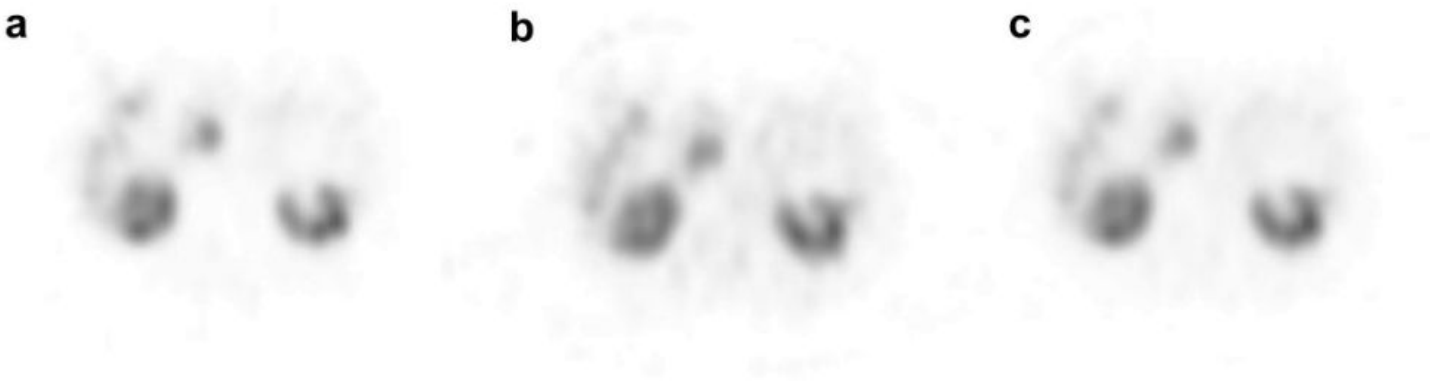

Figure 7

Images of a case with a tumor in the head of the pancreas; a 171 keV, b 245 keV, and c sum.

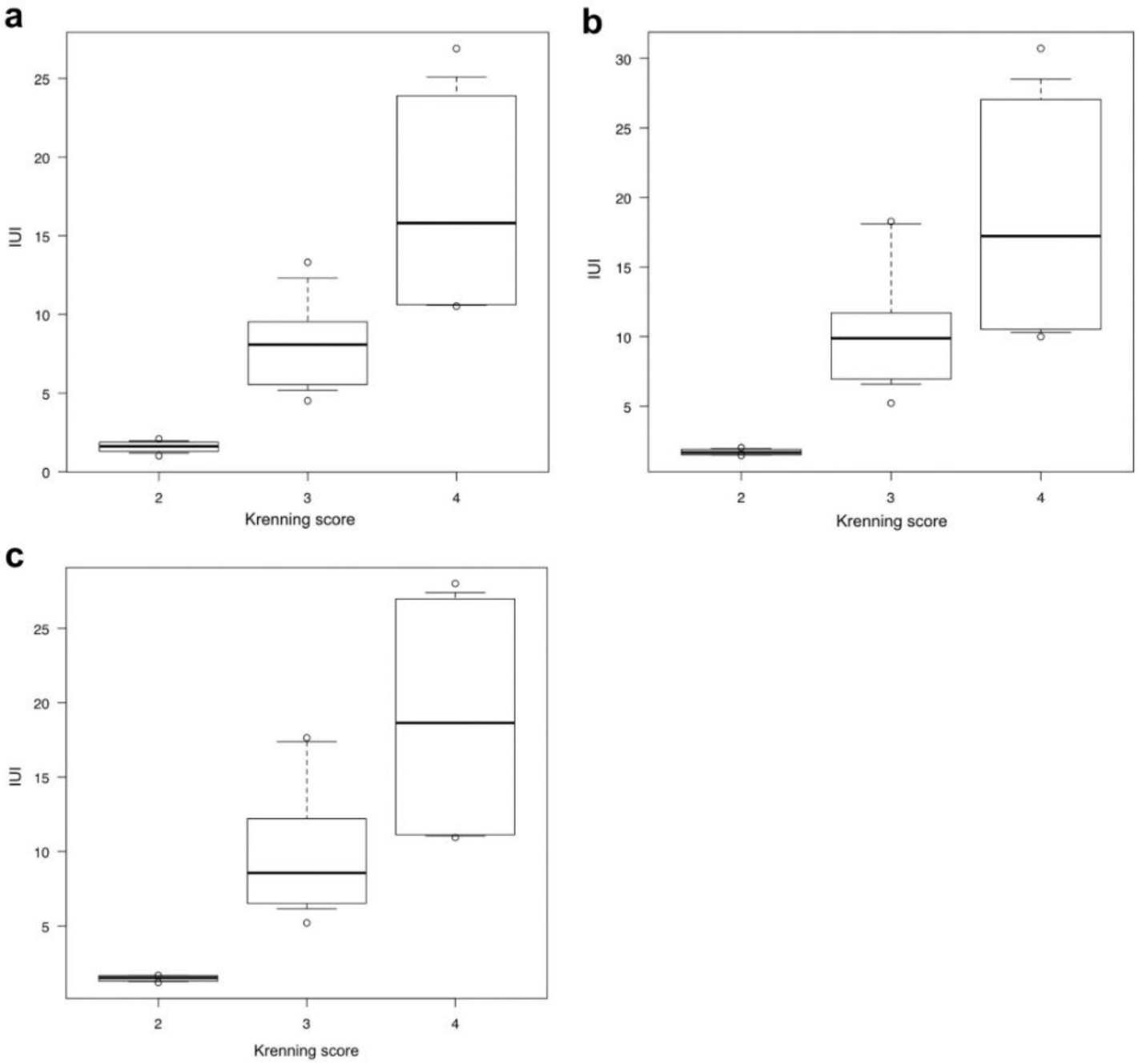

Figure 8

Boxplots showing the relationship between Krenning score and IUI in each window; a 171 keV, b 245 keV, and c sum.